Astron. Astrophys. 333, 313–321 (1998)

ASTRONOMY AND ASTROPHYSICS

Ideal kink instabilities in line-tied coronal loops

H. Baty[1], **G. Einaudi**[2], **R. Lionello**[3,4], **and M. Velli**[3]

[1] Observatoire Astronomique, 11 Rue de l'Université, F-67000 Strasbourg, France
[2] Dipartimento di Fisica, Università di Pisa, I-56100 Pisa, Italy
[3] Dipartimento di Astronomia e Science dello Spazio, Università di Firenze, I-50125 Firenze, Italy
[4] Science Applications International Corporation, San Diego, CA 92121-1578, USA

Received 7 November 1997 / Accepted 6 January 1998

Abstract. We investigate the nonlinear development of ideal kink instabilities in a line-tied coronal loop, using a three dimensional numerical code. In order to understand how the equilibrium loop properties affect nonlinear evolution, various different initial magnetic equilibria are considered. In most cases, a fine-scale magnetic field structure is shown to develop. However, the corresponding electric current structure depends sensitively on the initial equilibrium: the initial magnetic twist profile, the loop length, and the nature of the outer potential region. If there are resonant regions at the loop apex where the radial component of the linear perturbed magnetic field vanishes, a current concentration develops there in the subsequent non linear phase. Otherwise current concentrations may develop as a consequence of the effect of line-tying. The ensuing resistive evolution of the system and the impact on coronal activity are discussed.

Key words: Sun: corona – MHD – methods: numerical – instabilities

1. Introduction

The kink instability of coronal loops of different sizes may play a fondamental role in solar activity, initiating flares of different magnitudes and perhaps also contributing to the heating of the solar corona.

Coronal loops are magnetic flux tubes whose field lines are anchored in the dense photosphere where coronal perturbations are unable to affect the magnetic field. On the other hand, photospheric motions gradually induce electric currents in loops, leading to a winding of magnetic field lines and an increased energy content of the structure. It is well known that infinitely long current carrying laboratory diffuse pinches can be stabilized only by a proper inclusion of a radial, perfectly conducting wall (Newcomb 1960, Goedbloed 1971). On the Sun, it was conjectured that this stabilizing role should be played by the photospheric axial boundary conditions (Raadu 1972, Hood & Priest 1979). A proper treatment of boundary conditions showed that stabilization is indeed obtained, provided that, for a given loop length, the twist does not exceed a threshold (Hood & Priest 1979, Einaudi & Van Hoven 1983).

Once this threshold is exceeded however, an ideal kink instability develops. Given the small ratio of loop radius to length, toroidal curvature effects have traditionally been neglected, and we will follow the same approximation here, though we will discuss its limitations in the conclusion. Previous numerical results have shown the ability of the ideal kink mode to give rise to intense current gradients, for a few given unstable MHD equilibria (Strauss & Otani 1988, Craig & Sneyd 1990, Baty & Heyvaerts 1996, Baty 1997, Velli et al. 1997). The further effect of a non zero resistivity leads to the dissipation of magnetic energy, accompanied by reconnection of magnetic field lines (Einaudi et al. 1997). Recently, considering three different initial equilibria, Lionello et al. (1998) (hereafter referred to as Paper I) have shown that the electric current structure and an ensuing reconnection process depend sensitively on the initial magnetic configuration.

The aim of this paper is to extend the study of Paper I, by considering a wider variety of different magnetic field equilibria for the initial unstable loop configuration. We focus only on the first stage (i.e. the formation of the fine-scale current structure) for which resistivity can be neglected. We plan to study the effect of the resistivity in a future work. Moreover, we do not deal here with resistive kink or tearing instabilities (Velli et al. 1990b, Mok & Van Hoven 1982) for which resistivity has an important effect on stability limits and on the dynamics of the linear phase.

The linear properties of the kink mode are investigated using a stability code (Velli et al. 1990a), and numerical computations of the non linear evolution have been carried out using the full 3D MHD non linear evolution code, SCYL (Baty & Heyvaerts 1996).

The paper is organised as follows. The equilibrium classes are defined in Sect. 2. In Sect. 3, we present a stability study of the configurations considered in this work. The non-linear development of the kink instability is described in Sect. 4. Finally, in Sect. 5, we discuss the results emphasizing the dependence of linear eigen-mode structure and subsequent non linear density current distribution on equilibrium loop parameters. The consequences of an ensuing dissipative process, like magnetic

Send offprint requests to: H. Baty

reconnection, are also conjectured in the light of recent results obtained in Paper I and by Einaudi et al. (1997).

2. Equilibrium classes

In the following we will limit our discussion to cylindrically symmetric coronal loops and neglect toroidal curvature, a description which is justified by the large aspect ratio (i.e. ratio of loop length to radius) of loops in the solar corona. The solar loop is then represented by a cylindrical flux tube of length L, with footpoints of magnetic field lines anchored in the photosphere at two end-plates $z = \pm L/2$.

In the limit of a magnetically dominated solar corona, coronal loops are most probably best described via force-free equilibria:

$$\boldsymbol{J} \times \boldsymbol{B} = 0, \tag{1}$$

where $\boldsymbol{B}$ and $\boldsymbol{J}$ are the magnetic field and current density respectively.

Mikic et al. (1990) have calculated the equilibrium which result from an imposed localized photospheric flow acting on an initially potential axial magnetic field in cylindrical geometry. Though such equilibria are two dimensional with both radial and axial dependences, it is apparent from their results (Fig. 4 in the above quoted paper) that the equilibrium quantities are independent of the axial coordinate z over most of the loop length, except in narrow boundary layers near the photosphere. Moreover, Baty & Heyvaerts (1996) have shown that neglecting the axial dependence of the initial equilibrium has little effect on the stability of kink modes. Here we will therefore restrict ourselves to 1D equilibria, which are fully determined by the radial profile of one function, when considering force-free fields. This can be taken to be the magnetic twist angle Φ, which, for a flux tube of length L, when measured from $z = -L/2$ to $z = L/2$, is given by the following expression:

$$\Phi(r) = \frac{LB_\theta}{rB_z}, \tag{2}$$

with B_θ and B_z the azimuthal and axial components of the equilibrium magnetic field.

Depending on the radial variation of the twist, the different equilibria used in this study can be divided into three classes (hereafter A,B, and C), as shown in Fig. 1. Class A is defined by considering monotonically decreasing twist profiles, with a value ranging from a maximum in the central region (say on the axis) to zero at a radial distance, $r = c$, somewhere between the axis and the numerical boundary, at which location we assume a perfectly conducting wall. In practice this region is placed far enough away so as not to influence the dynamics. One can distinguish two physical regions in our equilibrium model: an internal one containing the current and an external potential region with a zero azimuthal magnetic field. Note also that, as a consequence of Ampere's law, the total current flowing in the loop is zero. Physically, these equilibria should result from a localized twisting photospheric flow acting on an initial potential magnetic configuration (Mikic et al. 1990).

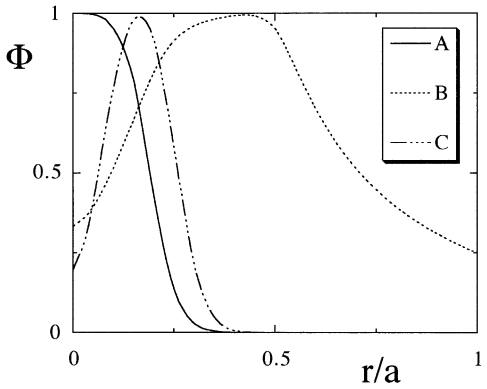

Fig. 1. Typical profiles of the magnetic twist for the three equilibrium classes considered.

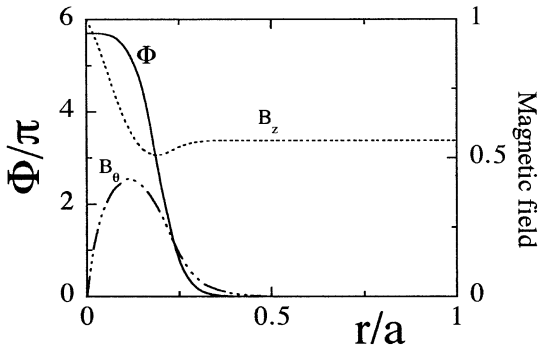

Fig. 2. The twist profile and the corresponding azimuthal and axial components of the magnetic field for equilibrium A1. The magnetic field is normalized to the value on the magnetic axis

In the second class (B), we consider monotonically increasing twist profiles in the inner region, with a minimum value of the twist on the axis and a maximum value near $r/a = 0.5$. The internal region is surrounded by a potential region between $r/a = 0.5$ and $r/a = 1$, where the twist decreases as $1/r^2$. Physically, these equilibria are more likely to result from an emerging magnetic structure through the photosphere in a non potential form.

Finally, class C includes non-monotonic twist profiles in the central region of the loop, and an external potential region with no twist and a purely axial magnetic field as in class A.

As in Paper I, all the magnetic configurations considered in this paper have the common property that the current is confined by an outer potential region. In terms of finiteness of the total current, we could also divide our equilibria into a null total axial current class (for cases A and C) and in a finite current class (case B), as in Paper I.

3. Linear stability

The stability of of a force-free field with uniform twist (Gold & Hoyle 1960) was first addressed by Raadu (1972) and subsequently Hood & Priest (1979). The Gold-Hoyle equilibrium (GH) is kink unstable when the twist value exceeds a critical value of 2.5π, or equivalently when the loop length exceeds a

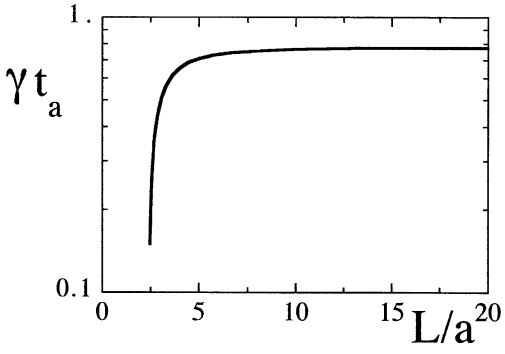

Fig. 3. The linear growth rate as a function of the length of the loop for equilibrium A1. The growth rate is normalized by the inverse Alfvén time $t_a^{-1} = v_a/a$, v_a being the Alfvén velocity on the axis.

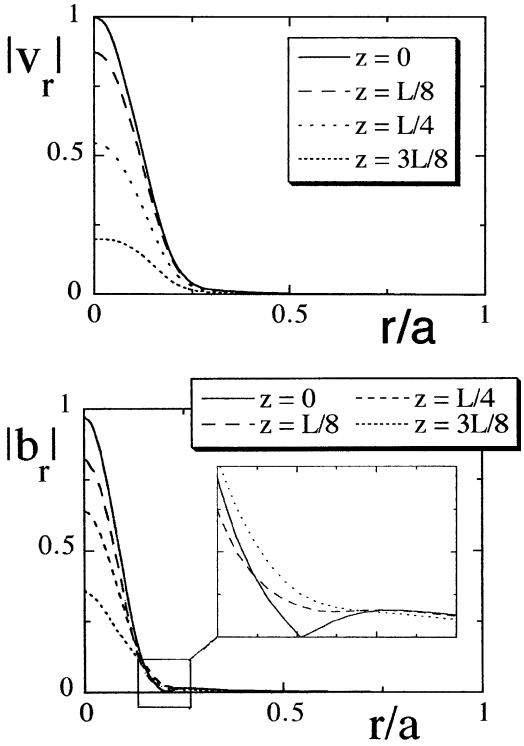

Fig. 4a and b Absolute values of the radial components of the velocity **a**, and of the perturbed magnetic field **b**, as a function of radius for equilibrium A1, at four different axial altitudes. Details of the magnetic field profiles in the vicinity of the resonant point are also shown.

critical value of $2.5\pi b$ (Hood & Priest 1979, Einaudi & Van Hoven 1983) as in this case we have a simple relation between the twist and the length of the loop $\phi = \frac{L}{b}$ (b being a characteristic radial length). This result demonstrates the stabilizing effect of line-tying, since the critical twist value for an axially periodic tokamak configuration is only 2π.

Although the GH equilibrium is of interest for understanding the basic physics, it is an overly simplified model for coronal loops. In more general cases, a simple expression for a critical twist no longer exists (the twist depends on radial distance, and one should then define an appropriate average twist, as discussed in Velli et al. 1990a). However, the stability limit can be expressed in terms of a critical loop length, which depends on the details of magnetic equilibrium. We have investigated the linear properties of the equilibria considered in Sect. 2, using a numerical stability code developped by Velli et al. (1990a). This numerical approach is based on Fourier series expansion for the displacement (Einaudi & Van Hoven 1981):

$$\boldsymbol{\xi}(\boldsymbol{r},t) = \boldsymbol{\xi}(\boldsymbol{r})\exp(\gamma t), \tag{3}$$

$$\boldsymbol{\xi}(\boldsymbol{r}) = \Re\sum_n \boldsymbol{\xi_n}(r)\exp[i(m\theta + n\pi(z/L+1))], \tag{4}$$

with γ the linear growth rate and we consider the $m = 1$ kink mode (m being the poloidal wavenumber). It has been shown that five axial Fourier harmonics centered around a central wavenumber are sufficient for an acceptable convergence of the sum in Eq. (4).

3.1. Class A

We have considered the initial equilibrium (A1) plotted in Fig. 2, where the radial position of the potential region is taken to be $c = 0.5a$. The corresponding azimuthal and axial magnetic field components, also plotted in Fig. 2, have been deduced solving numerically Eq. 1. The linear growth rate γ of the kink mode is shown in Fig. 3 as a function of the loop length. The critical length is $L_c/a = 2.35$. The linear mode structure is of fundamental importance in determining the subsequent non linear evolution of the instability. An important feature in this respect is the existence of a resonant point at the loop apex ($z = 0$), corresponding to the point where the radial component of the ideal perturbed magnetic field vanishes, and consequently where a non zero resistivity perturbation (i.e., a topology changing perturbation) may dominate the ideal one (Velli et al. 1990a). Moreover, intense current gradients are also expected to form in these regions during the non linear stage of the kink mode (Baty & Heyvaerts 1996).

Therefore, we have investigated the eigenfunctions of the kink mode at marginality (i.e. for a vanishing linear growth rate). Firstly, we have plotted the absolute value of the $m = 1$ radial component of the velocity as a function of the radial coordinate for different axial altitudes, as one can see in Fig. 4a. The results indicate that the radial velocity is essentially confined to the inner current region, with a very small contribution in the potential region. The perturbation is also maximum at the loop apex and minimum at the photosphere, a consequence of the line-tying effect. The absolute value of the $m = 1$ radial component of the perturbed magnetic field is also plotted in Fig. 4b. One can see that a resonant point exists, located at $r/a = 0.2$, at the loop apex. This site corresponds to a region where the corresponding radial velocity in Fig. 4a exhibits the strongest gradient. These results are in good agreement with those of Paper I, where the authors called the instability an internal kink mode for such magnetic configuration.

We have examined the effect of the position of the potential region, by varying c/a in the range [0.3:0.5] and keeping the

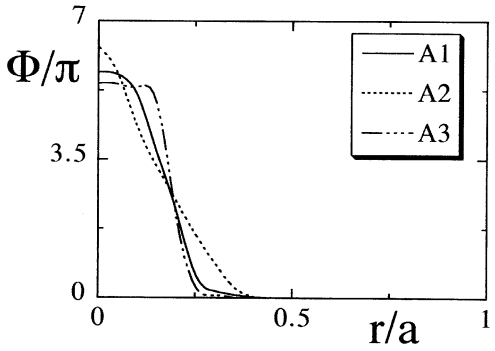

Fig. 5. The three equilibrium twist profiles A1, A2, and A3.

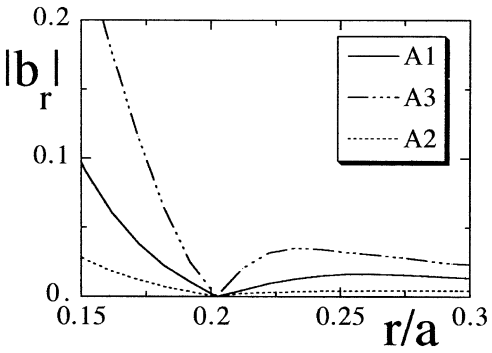

Fig. 6. The absolute values of the radial component of the perturbed magnetic field as a function of radius at the loop apex, for the three equilibria plotted in Fig. 5.

same twist profile (A1) in the vicinity of the resonant site: the results obtained, show that linear eigenfunctions are unaffected.

Secondly, we have examined the effect of magnetic shear (which is defined as the radial derivative of the twist) in the vicinity of the resonance, keeping c/a and the twist value at the resonant point constant. The twist profiles (A1-A2-A3) corresponding to the equilibria obtained are shown in Fig. 5. The values of the twist on the axis have been adjusted in order to keep the same critical length. The resulting magnetic field perturbations at the loop apex are plotted in Fig. 6. One can see that the equilibrium shear has an important effect on the steepness of the perturbation in the vicinity of the resonant point, the higher the shear the steeper the magnetic perturbation.

More precisely, we have obtained that the steepness varies proportionally to the shear.

We have also investigated the linear eigenfunctions for a given non zero linear growth rate, (i.e. far from the marginality) or equivalently for a loop length greater than the critical value. The results are similar to the marginal case.

3.2. Class B

Two different equilibria have been studied, as one can see in Fig. 7. The values of the twist have been chosen in order to give the same critical length as previously obtained for class A models, i.e. $L_c/a = 2.35$. Firstly, we have considered a uniform-twist-like equilibrium (B1), where the twist has a constant value

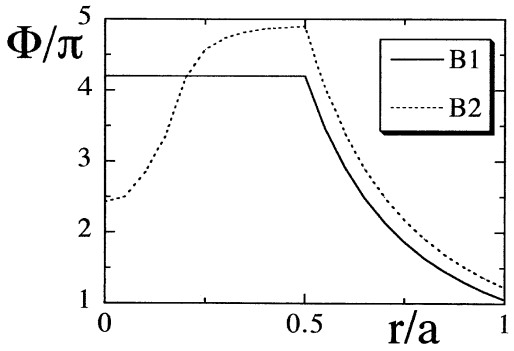

Fig. 7. The two equilibrium twist profiles B1 and B2.

in the inner plasma region situated between the axis $r = 0$ and $r/a = 0.5$. This is not the case for the second equilibrium (B2), where the twist is monotonically increasing from a mimimum value on the axis to a maximum at $r/a = 0.5$. In both cases, an outer potential region is situated between $r/a = 0.5$ and the numerical boundary $r/a = 1$, where the twist decreases as $1/r^2$. The resulting $m = 1$ radial components of the velocity and magnetic field perturbations at the loop apex are plotted in Fig. 8. Firstly, as one can see in Fig. 8b, a resonant point no longer exist. Secondly, the radial velocity is not confined to the inner current region, but retains a rather high value in the potential region (compared to previous results obtained for class A). An interesting comparison between equilibria B1 and B2 can also be made. Indeed, the effect of a variable twist in the inner region is to lead to non-monotonic magnetic and velocity perturbations. Moreover, for the same perturbation magnitude on axis, the maximum perturbation is higher for the variable twist case (B2).

This is in agreement with Paper I, where the finite current fields are shown to be subject to a global kink mode, which is characterized by a radial displacement not confined to the initial current region (contrary to a null current configuration).

3.3. Class C

As shown in Fig. 1, we have studied a non monotonic twist case surrounded by an outer potential region with a purely axial magnetic field. Again, the exact magnitude of the twist has been chosen to give the same critical length as in previous cases. The numerical results for the linear marginal eigenfunctions (radial velocity and radial magnetic field) at the loop apex are reported in Fig. 9. One can see that two resonant points are present. The first one is located in a region of positive magnetic shear, and the second one in a region of negative shear. The radial component of the velocity is also non monotonic, with a positive gradient coinciding with the first resonant site, and a negative gradient for the second site. Finally, the perturbation is confined to the inner loop region, as a consequence of the nature of this internal kink mode.

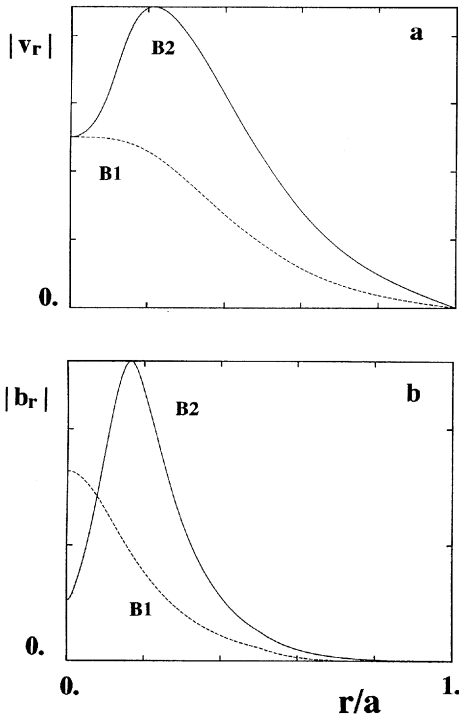

Fig. 8a and b The absolute values of radial velocity **a** and radial component of the perturbed magnetic field **b** as a function of radius at the loop apex, for the two equilibria plotted in Fig. 7.

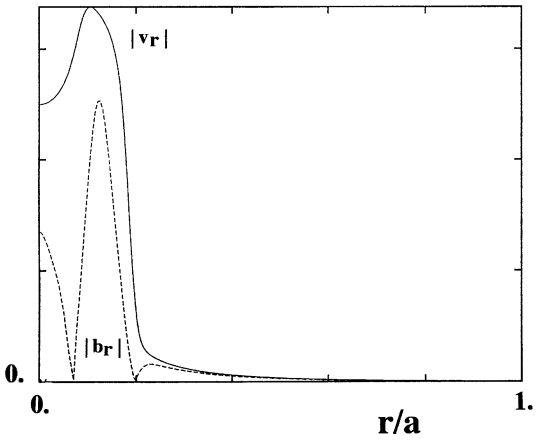

Fig. 9. The absolute values of radial velocity and radial component of the perturbed magnetic field, as a function of radius at the loop apex, for the class C equilibrium.

4. Nonlinear evolution

In order to investigate the nonlinear evolution of the different unstable configurations considered in this study, we have performed numerical simulations using the fully 3D cylindrical evolution code, SCYL (Baty & Heyvaerts 1996).

4.1. Physical model

SCYL solves the full set of compressible and viscous MHD equations, which can be written (in non-dimensional form):

$$\frac{\partial \rho}{\partial t} + \nabla \cdot (\rho \boldsymbol{v}) = 0, \tag{5}$$

$$\rho[\frac{\partial \boldsymbol{v}}{\partial t} + \boldsymbol{v} \cdot \nabla \boldsymbol{v}] = \boldsymbol{J} \times \boldsymbol{B} - \nabla P + \mu \triangle \boldsymbol{v}, \tag{6}$$

$$\frac{\partial P}{\partial t} + \boldsymbol{v} \cdot \nabla P = -\gamma P \nabla \cdot \boldsymbol{v} \tag{7}$$

$$\frac{\partial \boldsymbol{B}}{\partial t} = \nabla \times (\boldsymbol{v} \times \boldsymbol{B}), \tag{8}$$

$$\boldsymbol{J} = \nabla \times \boldsymbol{B}. \tag{9}$$

Here, ρ is the mass density, P the plasma pressure, $\boldsymbol{v}$ the fluid velocity, $\boldsymbol{B}$ the magnetic field, $\boldsymbol{J}$ the electric current desity. μ is the kinematic viscosity, and γ is the ratio of specific heats (a value 5/3 is used). The energy equation is as simplified as possible, describing only energy convection (Eq. 7) because the aim of the present simulation is to understand primarly the dynamics. It would be easy to modify Eq. (7) to include thermal conductivity, and we plan to do so in future work.

The MHD equations (5-9) are integrated in time using a second order semi-implicit scheme, which allows large time steps limited by the non linear physical plasma phenomena (Lerbinger & Luciani 1991). SCYL has proved its ability to simulate long time MHD evolution with a high spatial resolution in previous studies (Baty and Heyvaerts 1996, Baty 1997). Radially, finite differences on two staggered meshes are used. Variables are expanded in double Fourier series in θ and z and operations are performed using fast Fourier transform (FFT). We use 100 radial grid points with the possibility to accumulate in the vicinity of current layers. Indeed, the radial mesh is accumulated in the central current channel region and in the vicinity of resonant layers, where one expects current concentrations to develop. 24×128 grid points are used in $\theta \times z$ corresponding to 7 azimuthal modes ($m = 0, 1, ...7$) after de-aliasing (Aydemir & Barnes 1985), each with a band of 80 axial harmonics centered around the fastest growing one (Einaudi & Van Hoven, 1983).

4.2. Numerical procedure

To investigate the further non linear evolution of the different magnetic configurations considered in the previous section, in most cases we take a loop length $L/a = 2.67$ exceeding the critical length $L_c/a = 2.35$. Therefore, the equilibria are close to marginal stability but have sufficient linear growth rates to carry out reasonable simulations without excessive waste of cpu time. We start the simulations by adding a small $m = 1$ velocity perturbation of amplitude $v \sim 10^{-4}$ to the initial equilibrium considered. In order to save computer time and also to facilitate the comparison of time scales, the radial and axial profiles of the initial perturbation are derived from the linear results obtained with the stability code.

After a linear phase dominated by the $m = 1$ mode and characterized by a constant growth rate, $m > 1$ modes are non

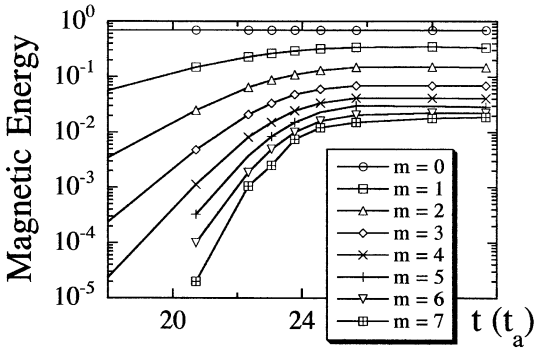

Fig. 10. Time history of the magnetic energy contained in the different m modes for an unstable A1 equilibrium

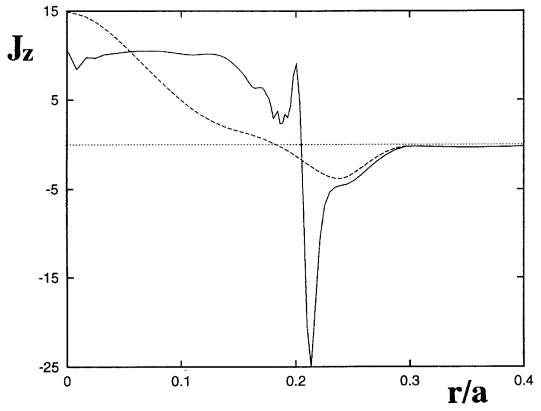

Fig. 11. The axial component of the current density at the loop apex ($z = 0$) for a given angle in the A1 case. The angle chosen is the one for which the current amplitude is maximum. Solid and dotted lines refer to the saturated kinked and initial configurations, respectively.

linearly driven via successive quadratric non linearities from the $m = 1$ mode. This non linear phase is illustrated in Fig. 10, where the time history of the magnetic energy contained in the different m modes is plotted for equilibrium A1. A similar time behaviour has been obtained for all the different equilibria studied in this work. Fig. 10 clearly shows that the nonlinear growth of $m > 1$ modes is followed by a saturation. This is in contrast with the results obtained in Paper I, where in all cases the end of the non-resistive phase corresponded to the onset of a numerical instability. This contrast is due to a different treatment of small scales in the two codes which introduces a different level of numerical dissipation. The problem of understanding whether the cascade towards small scales in reality proceeds to the formation of current sheets or is in some way stopped is beyond the scope of the present work and would need simulations carried out at much higher resolution. The important point here is that we can recognize the saturated state as the final state of the non-resistive phase discussed in Paper I. The non linear phase is followed using a rather small constant value for the viscosity coefficient $\mu = 10^{-3}$. We have checked that this value is an optimal one, as higher values lead to strong smoothing and smaller values to excessive use of computer time.

4.3. Class A

Firstly, we have examined the non linear evolution of the unstable A1 equilibrium. As previously shown (Baty & Heyvaerts 1996, Baty 1997), a current concentration non linearly develops at the resonant point at the loop apex, as one can see in Fig. 11 for the saturated state. Indeed, the radial location is near $r/a = 0.2$ in good agreement with the resonant site plotted in Fig. 4b. It appears as a negative contribution superposed on the initial density current. As shown in Fig. 12, this current concentration extends along all the loop length down to the photosphere, and takes the form of a helical ribbon of intense current. It's amplitude is maximum at the loop apex and minimum at the photosphere. Note that, even though we used the axial component of the current density as a diagnostic, the current structure obtained is similar for the other components. We have checked the non linear nature of the current concentration by showing that all m modes contribute to the current structure near the resonant point, eventhough the $m = 1$ mode is dominant. We have also checked that the position of the potential region has negligible effect on the described development of current structure. An important role, as in the linear phase, is played by magnetic shear. Indeed, comparison of results for the three cases (A1, A2, and A3) (as plotted in Fig. 13) shows that the amplitude of the saturated current concentration at the loop apex scales linearly with the shear of the initial equilibrium, the higher the shear, the stronger the amplitude of the current concentration. Similar results have been also obtained at other heights in the loop.

As mentioned previously, we have also examined the effect of distance from marginality, by performing a simulation with $L/a = 3.5$. The linear growth rate in his case is twice as large, compared to case A1. The results give an amplitude for the saturated current spike (measured at the loop apex) scaling approximately linearly with the loop length, in good agreement with Baty's results (1997). The localization of the current layer at the loop apex is little affected, though the helicity of the current concentration is higher, in correlation with the higher total twist of the equilibrium.

4.4. Class B

The non linear evolution of field B1 is remarkable for the absence of small scale formation in the magnetic and current structures even at saturation. The current-density is only redistributed in the loop, without developing intense gradients. This is in good agreement with previous results obtained for a uniform twist (Baty & Heyvaerts 1996), where an explanation in terms of the pathological nature of a constant twist profile was given. Indeed, a different behaviour is obtained for case B2: a helical current concentration is formed, as shown in Fig. 14, which, contrary to what occurs for fields of class A1, has the same sign as the initial density current (Fig. 15). It is situated in the inner current channel region, and is radially localized at the loop apex where the initial current density is maximum. As the resonant point no longer exists for this equilibrium, it can not be evoked to explain the localization of the current layer. However, a comparison be-

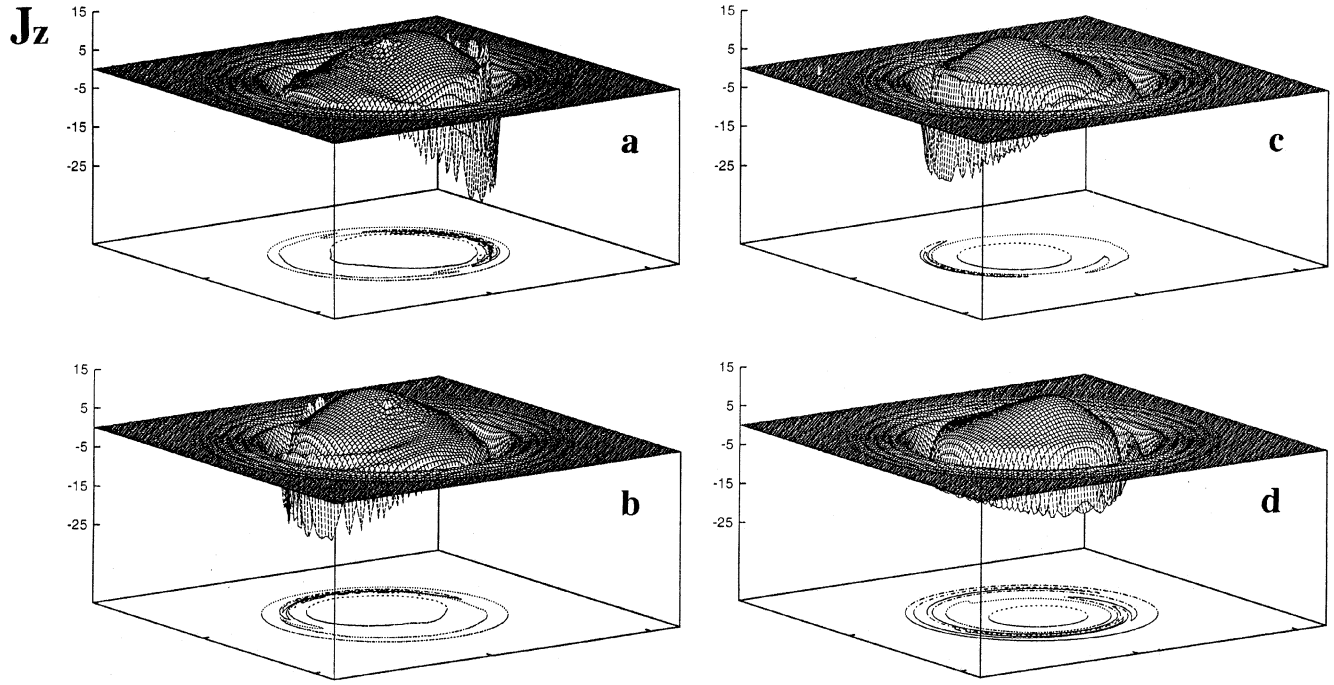

Fig. 12a–d The axial component of the current density for different axial altitudes $z = 0$ **a**, $z = L/8$ **b**, $z = L/4$ **c**, $z = 3L/8$ **d**, for the saturated A1 case.

tween the two cases (B1 and B2) leads us to the conclusion that the magnetic shear of the initial equilibrium has a primary role in the subsequent formation of current gradients. Indeed, the current layer region coincides with the maximum positive shear region of the initial equilibrium, and also with the region where the linear eigen-mode perturbations are maximum (Fig. 8).

Again, we have investigated the effect of the distance from marginality. The result is to change the localization of the current concentration and it's amplitude but not it's nature.

In Paper I, for a similar finite current equilibrium (labelled FC1 there) results on the current concentration which are somewhat different from those just described have been obtained. The FC1 results show that two current peaks develop, one per each half loop. And, the location of the current concentration also depends on the loop length. Even though the FC1 current concentrations are not maxima at the loop apex but approximately midway between the loop apex and the photosphere, their morphology is similar to the current structure developed in the B2 case. The differences are probably due to the extreme localization of the region of variable twist in the FC1 configuration, which results in a local magnetic shear which is two orders of magnitude higher than in the present configuration B2.

4.5. Class C

The saturated current structure obtained in this case exhibits two current peaks at the loop apex at different radii and opposite locations in the azimuthal angle, as seen from Fig. 16. While the second (negative) peak is clearly correlated to the existence of the second resonant site obtained in the linear study, the first

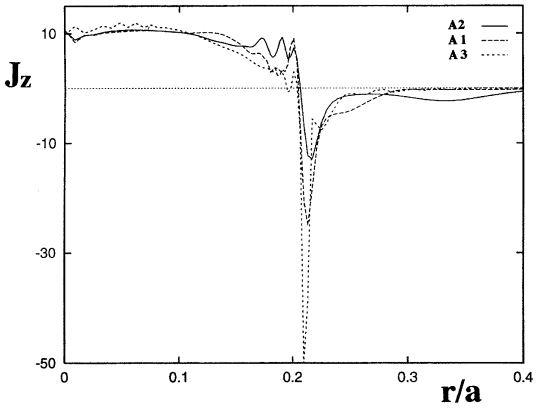

Fig. 13. Same as Fig. 11 for the A1, A2 and A3 cases.

(positive) peak is centered closer to the axis of the initial current channel rather than in the vicinity of the first resonant point.

For completeness, let us mention results concerning the instability of a final equilibrium profile, which has a twist profile similar to field A1, except that the inner current region between the axis $r = 0$ and $r/a = 0.3$ is connected to an outer potential region where the twist decreases as $1/r^2$. The aim of this simulation is to understand the effect of a potential region containing an azimuthal field. As concerns the linear mode structure, the results are similar to case A1, with a resonant point situated at $r/a = 0.2$, except that the radial displacement is more extended. The non-linear evolution of the kink configuration shows that the formation of current concentrations is also similar to the evolution obtained for class A fields, except that the current concentrations seem to invade the potential region.

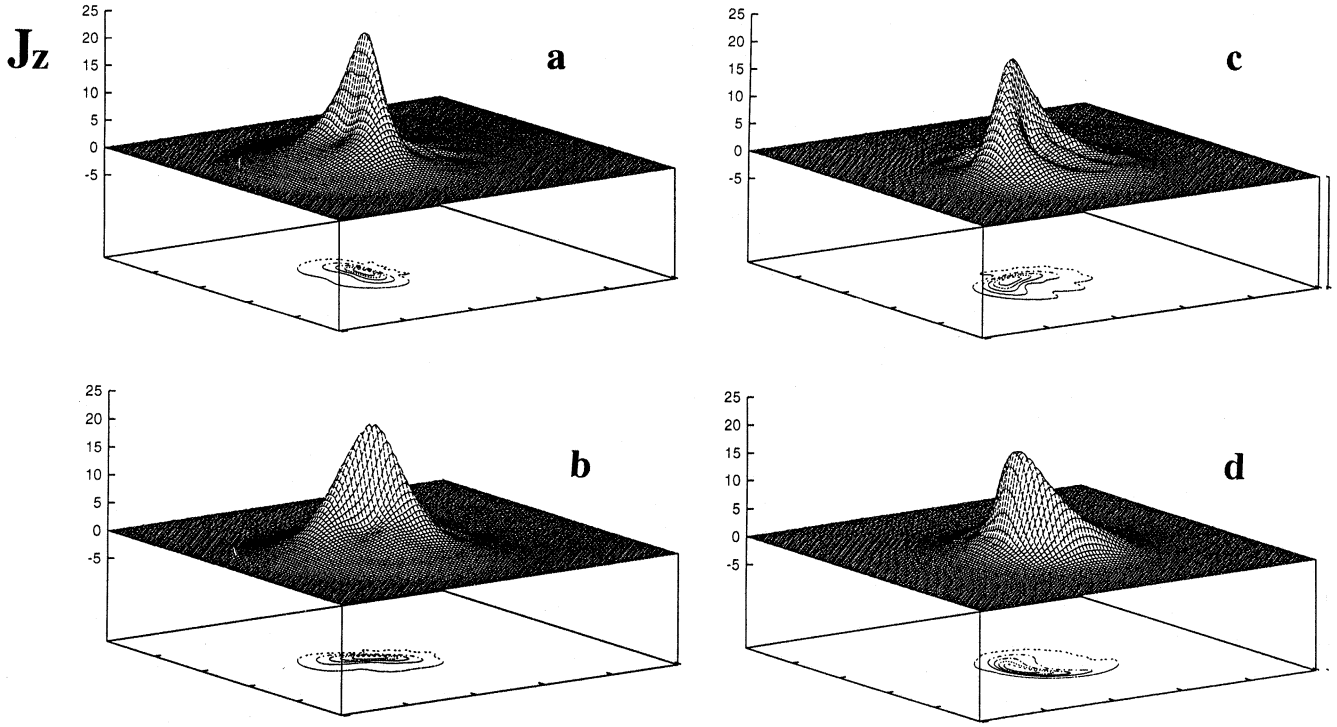

Fig. 14a–d Same as Fig. 12 for the B2 case.

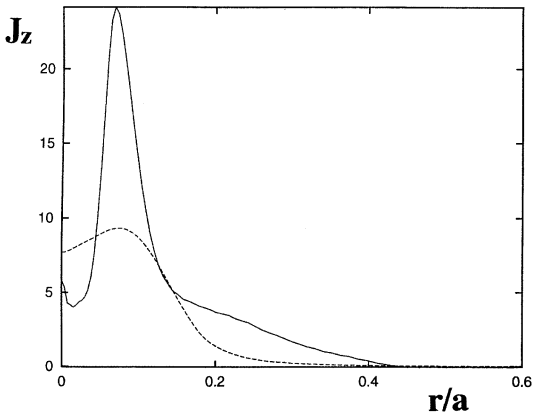

Fig. 15. Same as Fig. 11 for the B2 case.

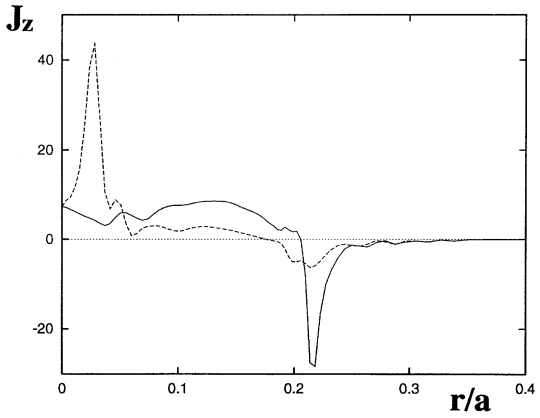

Fig. 16. The axial component of the current density at the loop apex ($z = 0$) for two angles in the saturated C cas e. The angles chosen are the ones for which the current amplitudes are maxima. They differ of π.

A similar case investigated in paper I, called FC2, led to the same conclusion.

5. Discussion

In this study, we have extended the results obtained in Paper I on the non-linear evolution of kink modes in line-tied coronal loops to a wider class of equilibrium field models. Firstly, we show that the alteration of magnetic field topology due to the kink instability depends sensitively on the parameters defining the initial unstable magnetic equilibrium, namely the twist profile (and associated shear profile) in the inner current region, the length of the loop, and the net axial current flowing in the loop.

More precisely, the radial variation of the twist in the innermost part of the loop is of fundamental importance in determining the nature of the current concentrations. Indeed, the presence of a resonant point at loop apex determines the position where one expects the development of a current concentration, especially for twist profiles having a negative magnetic shear (A class). The current peak appears then as a negative contribution superposed on the positive initial density current, and it extends helically along the loop length with a maximum amplitude at the loop apex. A current layer of different nature can also form without the presence of a resonance at the loop apex. This is the case for twist profiles having a positive magnetic shear in the

inner current region (B class). The current peak is positive (in correlation with the sign of the shear), and is situated where the current density was initially maximum.

A more complicated current structure is formed when the twist profile is non monotonic in the current region, as obtained for class C models.

We have also shown that the values of the shear and of the loop length are important in determining the magnitude and the localization of the current concentration.

Finally, the presence of an outer potential region where the magnetic field is purely axial helps confine the kink instability and consequently the current layer in the initial current region, as was previously shown in Paper I.

In order to describe the subsequent behaviour of all these kinked configurations, we should investigate the effect of a non-zero resistivity. As the current structure differs considerably from one equilibrium to the other, one expects different dissipative processes to be effective. The resistive evolution has been followed in Paper I, by setting a given (non-zero) value of the resistivity during the non linear stage of the development of the kink instability. They find that the final magnetic configuration and the amount of magnetic energy dissipated in the resistive phase depend sensitively on the initial magnetic configuration. Indeed, in the null current case (loop carrying a zero total axial current initially), exhibiting a resonant point at the loop apex, an unwinding of magnetic field lines occurs and the field has the tendency to become a potential one. A different behaviour is observed for the previously mentioned finite current case (FC1), where the reconnection involves field lines far in the potential outer region leading to an ergodic final configuration. However, since the order of magnitude of the FC1 twist is very high, resistive simulations of a wider variety of initial loop configurations are needed to extend the results presented in Paper I. We plan to do so, investigating the resistive evolution of the loop configurations considered in the present paper.

In order to assess the efficiency of the energy dissipation in the resistive phase of the evolution of kink instabilities and the impact of this process in coronal dynamics, it is of particular interest to determine the scaling of the reconnection process with resistivity. We plan to perform higher resolution simulations in the future to establish how the transverse dimensions of the current concentrations due to kink instabilities and the time scales of reconnection are modified at lower resistivity.

A final consideration concerning the geometric approximations used in this study must be made. Indeed, the effect of the loop toroidal curvature is presently not known and should be considered in future works. Recent simulation results (Amari et al. 1996) including the toroidicity of field lines in unconstrained geometry show a rapid expansion of the loop as it is twisted.

Acknowledgements. The numerical calculations were performed on the CRAY C98 at I.D.R.I.S., Orsay (France). This work was supported by the G.D.R. “Magnétodynamique solaire et stellaire”.

References

Amari T, Luciani J.F., Aly J.J., Tagger M., 1996, ApJ 466, L39
Aydemir A.Y., Barnes D.C., 1985, J. Comput. Phys. 59, 108,
Baty H., Heyvaerts J., 1996, A&A 308, 935
Baty H., 1997, A&A 318, 621
Craig I.J.D., Sneyd A.D., 1990, ApJ 357, 653
Baty H., 1997, A&A 318, 621
Einaudi G., Van Hoven G., 1981, Phys. Fluids 24, 1092
Einaudi G., Van Hoven G., 1983, Solar Phys. 88, 163
Einaudi G., Lionello R., Velli M., 1997, Adv. Space Res. 19, 1875
Goedbloed J.P., 1971, Physica 53, 501
Gold T., Hoyle F., 1960, MNRAS 120, 89
Hood A.W., Priest E.R., 1979, Solar Phys. 64, 303
Lerbinger K., Luciani, 1991, J. Comput. Phys. 97, 444
Lionello R., Velli M., Einaudi G., Mikic Z., 1998, ApJ, 494, in press (Paper I)
Mikic Z., Schnack D.D., Van Hoven G., 1990, ApJ 361, 690
Mok Y., Van Hoven G., 1982, Phys. Fluids 25, 636
Newcomb W.A., 1960, Ann. Phys. 10, 232
Raadu M.A., 1972, Solar Phys. 22, 425
Strauss H.R., Otani N.F., 1988, ApJ 326, 418
Velli M., Einaudi G., Hood A.W., 1990a, ApJ 350, 419
Velli M., Einaudi G., Hood A.W., 1990b, ApJ 350, 428
Velli M., Lionello R., Einaudi G., 1997, Solar Phys. 172, 257